Electronic polarizability effects on the anharmonic phonon shift and damping in ionic crystals

1992 J. Phys.: Condens. Matter 4 5291

(http://iopscience.iop.org/0953-8984/4/23/006)

J. Phys.: Condens. Matter 4 (1992) 5291–5300. Printed in the UK

Electronic polarizability effects on the anharmonic phonon shift and damping in ionic crystals

A Greco, S Koval and R Migoni

Departamento de Física, Facultad de Ciencias Exactas, Ingeniería y Agrimensura, (UNR) Instituto de Física Rosario (CONICET — UNR), Boulevard 27 de Febrero 210 Bis, 2000 Rosario, Argentina

Received 9 January 1992

Abstract. We apply a previously developed perturbative formalism for anharmonic shell models to the calculation of phonon shifts and widths in a simple one-dimensional model of a solid with polarizable ions. We analyse these properties for different k-points in the Brillouin zone and also as a function of temperature for fixed k. We compare our results for several values of the core–shell coupling constant g with those obtained by using a rigid-ion model ($g \to \infty$). We show that the electronic polarizability of ions leads to significant modifications of the k-dependences as well as of the ratio between the damping and shift. We give an interpretation of existing discrepancies between theory and experiment for anharmonic phonons in silicon. Finally, we mention some further applications.

1. Introduction

The shell model has been used with considerable success for the lattice dynamics of ionic crystals [1]. The outer electrons of the ions are represented in this model by spherically symmetric massless charge shells. In this way the polarizability effects are incorporated, and much better agreement than that predicted by the rigid-ion model can be achieved for the phonon dispersion curves as well as other observable material properties [2].

In the harmonic approximation the usual treatment is to solve for the shell coordinate from its equation of motion (adiabatic condition), and then to substitute it in, in order to obtain an effective potential for the motion of the cores (nuclei) [1].

The most important feature of the shell model is that the interactions involved have a direct physical interpretation. The effective couplings between cores, arising when the shell coordinates are eliminated, are generally complicated and difficult to find in the framework of a rigid-ion model.

However, in an anharmonic situation the shell coordinate cannot be obtained exactly from the adiabatic condition. This constraint generates implicitly anharmonic long-range effective interactions. Thus the formulation of the dynamics and statistical mechanics of the shell model with a general interaction potential requires careful treatment. A first approach in this direction was a perturbative formulation using a self-consistent phonon approximation as a generalization of the harmonic model [3]. More recently, a path-integral representation of the quantum partition function for a general adiabatic shell model was defined [4]. This was the starting point for a

0953-8984/92/235291+10$04.50

subsequent systematic development of a perturbation theory for the anharmonic shell model [5].

In this paper we show how this perturbative method applies to the calculation of the phonon shifts and dampings in a one-dimensional anharmonic shell model as a simple example of a system of an anharmonic crystal with polarizable ions. Our aim is also to compare the results with those obtainable from the model in the rigid-ion limit. Significant discrepancies will become apparent, thus showing the relevance of our formalism.

The paper is organized as follows. In section 2 the model is presented and the perturbative method of [5] is applied to it. In section 3 the numerical results and conclusions are given. Finally, in section 4 we present the discussion.

2. The model and perturbative method

With the aim of computing the phonon frequency corrections and lifetimes due to anharmonicities, we study the model defined by the following potential:

$$\Phi(u,v)=\sum_i\left(\tfrac{1}{2}f(v_i-v_{i-1})^2+\tfrac{1}{2}g(u_i-v_i)^2+\frac{f_3}{3!}(v_i-v_{i-1})^3+\frac{f_4}{4!}(v_i-v_{i-1})^4\right) \tag{2.1}$$

In equation (2.1), u_i and v_i are the core and shell displacements, respectively, at the site i. The quantities f and g are harmonic force constants, while f_3 and f_4 are cubic and quartic anharmonic constants, respectively (figure 1).

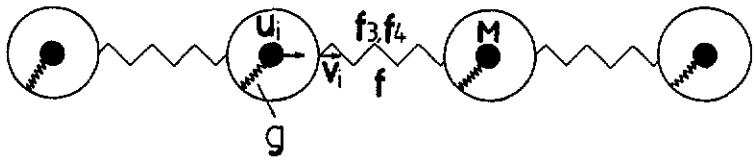

Figure 1. Monatomic chain of linearly polarizable ions with core–shell coupling constant g and harmonic, cubic and quartic shell–shell interactions f, f_3, f_4 between nearest neighbours. M is the ionic mass and u_i and v_i are the core and shell displacements, respectively, of the ith ion.

This model presents the main characteristics of an anharmonic shell model. For this reason most results obtained with this simple model will be qualitatively valid for general anharmonic shell models. Moreover, the model presents a well defined limit to the rigid-ion model. In the limit $g \to \infty$, where the ionic polarizability is neglected, we get a rigid-ion model with nearest-neighbour cubic and quartic interactions. Therefore, the phonon lineshifts and linewidths computed with the perturbation theory of [5] become the rigid-ion model values [6].

The potential can be written in a more compact form:

$$\Phi(u,v)=\tfrac{1}{2}R_{ij}u^iu^j+T_i^ju^iv_j+\tfrac{1}{2}S^{ij}v_iv_j+(1/4!)F_4^{ijkl}v_iv_jv_kv_l+(1/3!)F_3^{ijk}v_iv_jv_k \tag{2.2}$$

where the matrix elements can be found in appendix 1.

From here on, we shall use the notation and results of [5]. Using

$$\partial\Phi/\partial v = Tu + Sv + (1/3!)F_4vvv + (1/2!)F_3vv \tag{2.3}$$

$$\partial\Phi/\partial v\partial v = S + (1/2!)F_4vv + F_3v \tag{2.4}$$

and the vector

$$\boldsymbol{X} = \begin{vmatrix} u \\ v \\ \lambda \end{vmatrix} \tag{2.5}$$

the effective action S' takes the form

$$S' = \tfrac{1}{2}X^\alpha G^{-1}_{\alpha\beta}X^\beta + \eta^* S\eta + (1/4!)A^{(4)}_{\alpha\beta\gamma\delta}X^\alpha X^\beta X^\gamma X^\delta + (1/3!)A^{(3)}_{\alpha\beta\gamma}X^\alpha X^\beta X^\gamma + B^{(3)}_\alpha X^\alpha \eta^*\eta + (1/2!)B^{(4)}_{\alpha\beta}X^\alpha X^\beta \eta^*\eta \tag{2.6}$$

where, in order to use the simplified diagrammatic rules [5], all the italic indices are suppressed. The only non-vanishing matrix elements in (2.6) are

$$A^{(4)}_{2222} = A^{(4)}_{3222} = A^{(4)}_{2322} = A^{(4)}_{2232} = A^{(4)}_{2223} = F_4 \tag{2.7a}$$

$$A^{(3)}_{222} = A^{(3)}_{322} = A^{(3)}_{232} = A^{(3)}_{223} = F_3 \tag{2.7b}$$

$$B^{(4)}_{22} = F_4 \tag{2.7c}$$

$$B^{(3)}_2 = F_3. \tag{2.7d}$$

Besides the terms with the propagators $G_{\alpha\beta}$ and S^{-1} (see [5]) in the effective action (2.6), we have four terms with different types of vertices:

$(-1)(1/4!)A^{(4)}_{\alpha\beta\gamma\delta}$: 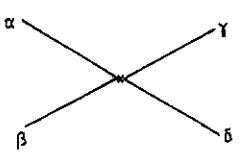

(2.8a)

$(-1)(1/3!)A^{(3)}_{\alpha\beta\gamma}$: 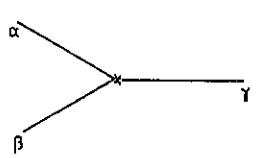

(2.8b)

$(-1)(1/2!)B^{(4)}_{\alpha\beta}$: 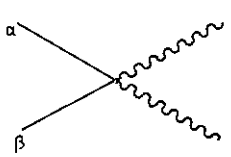

(2.8c)

$(-1)B^{(3)}_\alpha$: 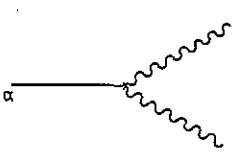

(2.8d)

The diagrams with two external legs containing up to two vertices of type F_3 and diagrams with one vertex of type F_4 are

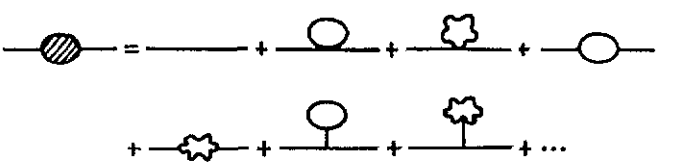

(2.9)

Diagrams with two vertices F_3 and diagrams with one vertex F_4 are in the same order of perturbation theory [7]. Using the diagrammatic rules [5] and reinserting italic indices, we obtain

$$= g_{ij} - \tfrac{1}{2} g_{iq} X^{(4)}_{(qklm)} g_{kl} g_{mj} + \tfrac{1}{2} g_{iq} X^{(3)}_{(qlp)} g_{lt} g_{ph} X^{(3)}_{(ths)} g_{sj}$$
$$+ \tfrac{1}{2} g_{iq} X^{(3)}_{(qlp)} g_{pt} g_{hs} X^{(3)}_{(ths)} g_{lj} + \tfrac{3}{2} g_{iq} Z_{(qklm)} g_{kl} g_{mj} \qquad (2.10)$$

where

$$X^{(4)}_{jklm} F_4^{npqr} S^{-1}_{nt} S^{-1}_{ps} S^{-1}_{qi} S^{-1}_{rv} T^t_j T^s_k T^i_l T^v_m \qquad (2.11a)$$

$$X^{(3)}_{jkl} = F_3^{npq} S^{-1}_{nt} S^{-1}_{ps} S^{-1}_{qi} T^t_j T^s_k T^i_l \qquad (2.11b)$$

$$Z_{twxa} = F_3^{ijk} S^{-1}_{il} F_3^{lph} S^{-1}_{jq} S^{-1}_{kx} S^{-1}_{py} S^{-1}_{hb} T^q_t T^x_w T^y_z T^b_a . \qquad (2.11c)$$

The parentheses mean that the expression has been symmetrized in all the enclosed indices.

Using the expressions in appendix 1 for the matrices, equations (2.10) in the reciprocal space lead us to the following free-phonon frequency correction Δ (to the harmonic dispersion curve $\omega^0(q)$) and inverse of the phonon lifetime Γ:

$$\Delta(k,\omega) = \Delta^{(1)}(k,\omega) + \Delta^{(2)}(k,\omega) + \Delta^{\mathrm{NEW}}(k,\omega) \qquad (2.12)$$

where

$$\Delta^{(1)}(k,\omega) = 2 f_4 \frac{\hbar}{8NM^2} \frac{\gamma^2(k)}{\omega^0(k)} g^4 \sum_q \frac{\gamma^2(q)}{\omega^0(q)} H^{(1)}(k,q)(2n_q + 1) \qquad (2.13a)$$

$$\Delta^{(2)}(k,\omega) = -\frac{1}{16} \frac{\hbar f_3^2}{NM^3} g^6 \frac{\gamma^2(k)}{\omega^0(k)} \sum_{q_1 q_2} \frac{\gamma^2(q_1)\gamma^2(q_2)}{\omega^0(q_1)\omega^0(q_2)}$$
$$\times \Delta(K - q_1 - q_2) H^{(2)}(k, q_1, q_2) P(\omega, \omega_1^0, \omega_2^0) \qquad (2.13b)$$

$$\Delta^{\mathrm{NEW}}(k,\omega) = -f_3^2 \frac{\hbar}{NM^2} \frac{\gamma^2(k)}{\omega^0(k)} g^4 \sum_q \frac{\gamma(k+q)\gamma^2(q)}{\omega^0(q)}$$
$$\times [\sin(k+q)a - \sin(ka) - \sin(qa)]^2 (2n_q + 1) \qquad (2.13c)$$

and

$$\Gamma(k,\omega) = \frac{\pi\hbar f_3^2}{16NM^3}g^6\frac{\gamma^2(k)}{\omega^0(k)}\sum_{q_1q_2}\frac{\gamma^2(q_1)\gamma^2(q_2)}{\omega^0(q_1)\omega^0(q_2)}\Delta(k-q_1-q_2)$$
$$\times H^{(2)}(k,q_1,q_2)D(\omega,\omega_1^0,\omega_2^0). \tag{2.14}$$

All the expressions belonging to (2.13) and (2.14) can be found in appendix 2.

The contribution to Δ from the diagram:

is zero because of the inversion symmetry [6].

The term Δ^{NEW}, in equation (2.12), is due only to our formalism. When performing the perturbation theory up to second order in f_3, a quartic vertex appears with two F_3 and one S^{-1} (see the last term in (2.10)).

It is easy to see that, when $g \to \infty$, $\Delta^{(2)}$ and $\Delta^{(1)}$ tend to the corrections of the dispersion curves corresponding to the rigid-ion model with cubic and quartic nearest-neighbour interactions given by force constants f_3 and f_4, respectively. On the other hand, Δ^{NEW} vanishes in this limit.

3. Results and conclusions

Using the results of section 2, we computed numerically the frequency shift $\Delta(k,\omega)$ (equation (2.12)) and damping constant $\Gamma(k,\omega)$ (equation (2.14)). For this purpose, the sum over q was evaluated by using 100 points of the Brillouin zone. The contribution of the Umklapp processes had to be taken into account in this procedure. We have chosen the Gaussian representation of the δ-function:

$$\delta(w) = \lim_{\epsilon\to 0}\left[(1/\epsilon\sqrt{\pi})\exp(-\omega^2/\epsilon^2)\right] \tag{3.1}$$

while for the principal part of Δ we have taken the following expression:

$$(1/x)_p = \lim_{\epsilon\to 0}[x/(x^2+\epsilon^2)] \tag{3.2}$$

with values of ϵ small but finite. The numerical values of Δ and Γ which result are almost independent of ϵ over a range of values. We select the value of ϵ in the centre of such range. In this way, we obtain $\epsilon_\Gamma = 0.6872$ THz for the δ-representation and $\epsilon_\Delta = 0.000\,098\,2$ THz for the principal-part representation.

Table 1. Parameters of the model

M (amu)	f (eV Å^{-2})	f_3 (eV Å^{-3})	f_4 (eV Å^{-4})
120.5	0.156 25	−0.072 25	0.006 25

Table 2. Different contributions to the lineshift Δ for $g = 3f$ (upper values) and for the rigid-ion limit $g \to \infty$ (lower values) at $T = 500$ K. $\Delta_N^{(2)}$ and $\Delta_U^{(2)}$ are the normal and Umklapp contributions to $\Delta^{(2)}$. Δ^T is the total lineshift. We give the values of Δ at different k-points of the Brillouin zone.

k (units of π/a)	$\Delta^{(1)}$ (THz)	$\Delta_N^{(2)}$ (THz)	$\Delta_U^{(2)}$ (THz)	Δ^{NEW} (THz)	Δ^T (THz)
0.20	0.0077	−0.0954	−0.0008	−0.0233	−0.1117
	0.0171	−0.2623	−0.0093	−0.0000	−0.2545
0.40	0.0094	−0.0835	−0.0023	−0.0328	−0.1092
	0.0325	−0.4799	−0.0372	−0.0000	−0.4846
0.60	0.0085	−0.0536	−0.0045	−0.0340	−0.0835
	0.0447	−0.6272	−0.0845	−0.0000	−0.6670
0.80	0.0076	−0.0350	−0.0081	−0.0331	−0.0686
	0.0525	−0.6807	−0.1560	−0.0000	−0.7841
1.00	0.0073	−0.0154	−0.0154	−0.0327	−0.0561
	0.0552	−0.2908	−0.2908	−0.0000	−0.5264

For the numerical evaluation of our expressions we choose the model parameter values shown in table 1, which give frequencies in the terahertz range and phonon shifts and widths within a few per cent of the bare phonon frequencies.

We perform the calculations for several values of the core–shell coupling g. This is the relevant parameter of the shell model and, as explained in the previous section, the limit $g \to \infty$ will allow us to consider the rigid-ion behaviour.

In table 2, we compare the different contributions to the lineshift Δ for $g = 3f$ with those for $g \to \infty$ at $T = 500$ K. The same comparison is made for the linewidth 2Γ in table 3. With the chosen ratio $g/f = 3$ which is quite reasonable in shell model calculations, we observe in tables 2 and 3 that the values of Δ and Γ are substantially smaller than those for $g \to \infty$. This is the first indication that the anharmonic parameters determined in the framework of a rigid-ion perturbation theory cannot be employed in a shell model where the short-range interactions are supposed to act between shells of neighbouring ions.

We compute the ratio Δ_{SM}/Δ_{RI} of the total lineshift of the shell model (with finite g) to the total lineshift of the rigid-ion model ($g \to \infty$) at $T = 500$ K. In figure 2 we show Δ_{SM}/Δ_{RI} as a function of the wavevector k throughout the Brillouin zone and for different values of g.

An analogous analysis of the linewidth ratio $2\Gamma_{SM}/2\Gamma_{RI}$ is made in figure 3.

Both ratios are strongly k-dependent even for the reasonable value $g = 3f$. The shell model quantities lie below the rigid-ion values and the differences increase towards the Brillouin zone boundary. This behaviour is understandable by considering that the shell displacement amplitude grows for modes with increasing k. Thus the attenuation of the inter-ionic spring stretching due to shell–core displacements is more marked near the zone boundary. The less the springs are stretched, the smaller are the anharmonic effects. A value $g = 10f$ produces a zone boundary frequency only 8.7% below that of the rigid-ion model, while the shell model lineshift and linewidth are still about 60% smaller than rigid-ion values, as seen in figures 2 and 3 at $k = \pi/a$. The differences between the shell model and rigid-ion model results become negligible only for very high values of g, about two orders of magnitude higher than the inter-ionic force constant f.

Let us now consider the temperature dependences at the zone boundary and

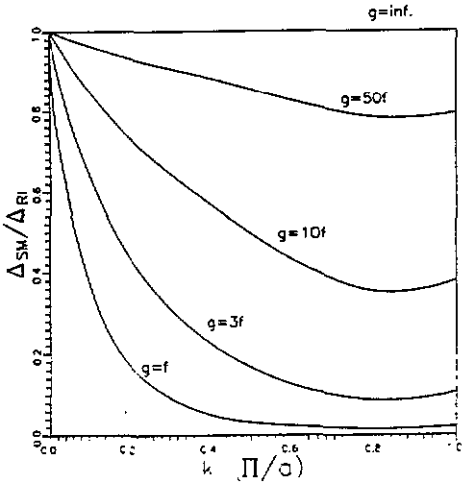

Figure 2. The ratio Δ_{SM}/Δ_{RI} of the total lineshift of the shell model to the corresponding lineshift of the rigid-ion limit versus wavevector k along the Brillouin zone. We plot the ratio for different values of g at $T = 500$ K.

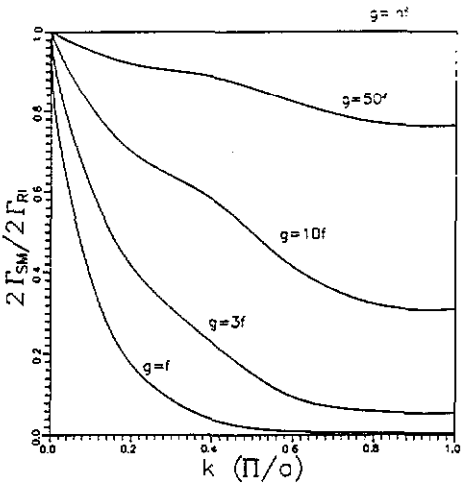

Figure 3. The ratio $2\Gamma_{SM}/2\Gamma_{RI}$ of the linewidth of the shell model to the corresponding linewidth of the rigid-ion limit versus wavevector k along the Brillouin zone. We plot the ratio for different values of g at $T = 500$ K.

Table 3. Different contributions to the linewidth 2Γ for $g = 3f$ (upper values) and for the rigid-ion limit $g \to \infty$ (lower values) at $T = 500$ K. $2\Gamma_N$ and $2\Gamma_U$ are the normal and Umklapp contributions to 2Γ. $2\Gamma^T$ is the total linewidth. We give the values of 2Γ at different k-points of the Brillouin zone.

k (units of π/a)	$2\Gamma_N$ (THz)	$2\Gamma_U$ (THz)	$2\Gamma^T$ (THz)
0.20	0.0851	0.0000	0.0851
	0.2046	0.0000	0.2046
0.40	0.1496	0.0000	0.1496
	0.6612	0.0000	0.6612
0.60	0.1128	0.0000	0.1128
	1.1932	0.0000	1.1932
0.80	0.0756	0.0001	0.0757
	1.2714	0.0018	1.2732
1.00	0.0354	0.0354	0.0709
	0.6418	0.6418	1.2836

compare again the rigid-ion behaviour with the shell model behaviour. We observe in equations (2.12)–(2.14) that the value of g does not affect the behaviour of Δ and Γ as functions of temperature. Therefore the ratios $[\Delta(T) - \Delta(0)]_{SM}/[\Delta(T) - \Delta(0)]_{RI}$ and $\Gamma_{SM}(T)/\Gamma_{RI}(T)$, shown in table 4 for different values of g, are independent of T.

Note that the Γ-ratios are significantly smaller than the Δ-ratios. This implies that the ratio of the linewidth to the lineshift of the zone boundary phonon is smaller for the shell model than for the rigid-ion model. The same applies to most k-values. Therefore, in general, if the anharmonic force constants are adjusted to fit phonon shifts, the linewidths are expected to have smaller values when the anhar-

Table 4. Values of the T-independent ratios $[\Delta(T)-\Delta(0)]_{SM}/[\Delta(T)-\Delta(0)]_{RI}$ and $\Gamma_{SM}(T)/\Gamma_{RI}(T)$ at the zone boundary for several values of the core–shell coupling constant g.

g	$[\Delta(T)-\Delta(0)]_{SM}/[\Delta(T)-\Delta(0)]_{RI}$	$\Gamma_{SM}(T)/\Gamma_{RI}(T)$
f	0.0213	0.0046
$3f$	0.1071	0.0552
$10f$	0.3796	0.3101
$50f$	0.7934	0.7632
$\rightarrow\infty$	1.0000	1.0000

monic interactions connect polarizable ions than in the case when they are considered between effectively rigid ions. The former case is properly treated in our formalism.

4. Discussion

The harmonic shell model has been used since 1960 to describe accurately the phonon dispersion curves of many compounds at a fixed temperature. In the cases where the anharmonic effects have also been studied, however, a perturbation theory based on a development of the crystal potential in higher orders of the nuclear displacements has been employed. The bare phonon frequencies calculated with the shell model are used in the expressions in [6] for the lineshifts and linewidths corresponding to such anharmonic theory. Therefore, although the long-range interactions generated by the polarization of the electronic shells through the adiabatic condition are taken into account in the harmonic approximation, they are neglected when incorporating anharmonicities. These are taken for effectively rigid ions.

In the present work we have shown that a consistent perturbative treatment of the anharmonic interactions in a shell model [5] leads to substantial qualitative and quantitative differences from the former treatment. Firstly, the anharmonic parameters necessary to explain a given phonon shift and width are larger for the shell model than for the rigid-ion model. Secondly, the shell model gives a different (generally smaller) ratio of linewidth to lineshift. Thirdly, both features are k-dependent.

The second fact mentioned above enables us to give a possible interpretation of the discrepancies found by Cowley [8] in the treatment of the anharmonicities in silicon. Cowley described the harmonic dispersion curves for silicon using a shell model. Then he followed the procedure described at the beginning of this section to calculate the lineshift and linewidth of the optical phonon at the Brillouin zone centre. He reproduced satisfactorily the phonon lineshift but predicted values much larger than the experimental data for the phonon linewidth. The origin of these discrepancies has recently been the subject of speculation [9]. Our results show that they may be ascribed to the neglect of the polarizability effects in the treatment of anharmonicities. We shall pursue a detailed analysis of this problem in future work.

We are also interested in the tetragonal-to-orthorhombic phase transition that takes place in La_2CuO_4. By starting from a shell model fit of the phonon dispersion curves [10], we shall analyse the soft mode responsible for the structural transition by using the shell model perturbation theory [5] as described in this work. Moreover, we shall try to compare the evaluation with that recently carried out in the framework of a rigid-ion model [11]. It is also interesting to study, with a shell model for

La_2CuO_4, the role played by a non-linear oxygen polarizability in the structural transition mentioned above. This anharmonic behaviour of the oxygen polarizability was used to explain the phase transition in recent work [12].

Acknowledgments

The authors are grateful to A Dobry and M Stachiotti for helpful discussions. AG acknowledges support from CIUNR. SK and RM acknowledge support from Consejo Nacional de Investigaciones Científicas y Técnicas.

Appendix 1

The non-vanishing matrix elements in (2.2) are

$$R_{ij} = g \qquad \text{if } i = j \tag{A1.1}$$

$$T_i^j = -g \qquad \text{if } i = j \tag{A1.2}$$

$$S^{ij} = \begin{cases} (2f+g) & \text{if } i = j \\ -f & \text{if } j = i-1, \text{ and index permutations} \end{cases} \tag{A1.3}$$

$$F_4^{ijkl} = \begin{cases} 2f_4 & \text{if } i=j=k=l \\ -f_4 & \text{if } i=j=k=l+1, \text{ and index permutations} \\ f_4 & \text{if } i=j, k=l=i-1, \text{ and index permutations} \\ -f_4 & \text{if } i=j=k=l-1, \text{ and index permutations} \end{cases} \tag{A1.4}$$

$$F_3^{ijk} = \begin{cases} -f_3 & \text{if } j=k=l+1, \text{ and index permutations} \\ f_3 & \text{if } i=j+1=k+1, \text{ and index permutations.} \end{cases} \tag{A1.5}$$

Appendix 2

In equation (2.13*a*) we have

$$H^{(1)}(k,q) = 2 + \cos[(k+q)a] + \cos[(k-q)a] - 2\cos(ka) - 2\cos(qa) \tag{A2.1}$$

where a is the lattice constant, while in (2.13*b*) we have

$$\begin{aligned} H^{(2)}(k,q_1,q_2) = {} & \{\cos(ka) + \cos(q_1a) + \cos(q_2a) - \cos[(k-q_1)a] \\ & - \cos[(k-q_2)a] - \cos[(q_1+q_2)a]\}^2 + \{-\sin(ka) + \sin(q_1a) \\ & + \sin(q_2a) + \sin[(k-q_1)a] + \sin[(k-q_2)a] - \sin[(q_1+q_2)a]\}^2 \end{aligned} \tag{A2.2}$$

and

$$\begin{aligned} P(\omega,\omega_1^0,\omega_2^0) = {} & [(n_1+n_2+1)/(\omega+\omega_1^0+\omega_2^0)_P - (n_1+n_2+1)/(\omega-\omega_1^0-\omega_2^0)_P \\ & + (n_1-n_2/(\omega-\omega_1^0+\omega_2^0)_P - (n_1-n_2)/(\omega+\omega_1^0-\omega_2^0)_P]. \end{aligned} \tag{A2.3}$$

In (2.14) we have

$$D(\omega,\omega_1^0,\omega_2^0) = (n_1+n_2+1)\left[\delta(\omega-\omega_1^0-\omega_2^0)-\delta(\omega+\omega_1^0+\omega_2^0)\right] + (n_1-n_2)\left[\delta(\omega+\omega_1^0-\omega_2^0)-\delta(\omega-\omega_1^0+\omega_2^0)\right]. \tag{A2.4}$$

Other important definitions are

$$\gamma(q) = [(2f+g)-2f\cos(qa)]^{-1} \tag{A2.5}$$

$$\omega^0(q) = \{[2f\sin^2(qa/2)]/[1+(2f/g)\sin^2(qa/2)]\}^{-1/2} \tag{A2.6}$$

$$n_q = \{\exp[\beta\hbar\omega^0(q)]-1\}^{-1}. \tag{A2.7}$$

In (A2.3) the suffix P denotes principal part, while in (2.13) and (2.14) the Δ-function reflects wavevector conservation, modulo a reciprocal lattice vector.

The notation ω_i^0 means $\omega^0(q_i)$, while n_i means n_{q_i}.

References

[1] Cochran W 1971 *Crit. Rev. Solid State Sci.* **2** 1
[2] Woods A, Cochran W and Brockhouse D 1960 *Phys. Rev.* **119** 980
[3] Ball R 1986 *J. Phys. C: Solid State Phys.* **19** 1293; 1989 *Ionic Solids at High Temperatures* ed A M Stoneham (Singapore: World Scientific)
[4] Dobry A and Greco A 1990 *J. Phys. A: Math. Gen.* **23** 567
[5] Dobry A, Greco A and Zandron O 1991 *Phys. Rev.* B **43** 1084
[6] Maradudin A A and Fein A E 1962 *Phys. Rev.* **128** 2589
[7] Califano S, Schettino V and Neto N 1981 *Lattice Dynamics of Molecular Crystals* (Berlin: Springer)
[8] Cowley R 1965 *J. Physique* **26** 659
[9] Haro E, Balkanski M, Wallis R and Wanser K 1986 *Phys. Rev.* B **34** 5358
Narasimhan S and Vanderbilt D 1991 *Phys. Rev.* B **43** 4541
[10] Koval S, Migoni R and Bonadeo H 1992 *J. Phys.: Condens. Matter* **4** 4759
[11] Heid R and Rietschel H 1991 *Phys. Rev.* B **44** 734
[12] Bussman-Holder A, Migliori A, Fisk Z, Sarrao J, Leisure R and Cheong S 1991 *Phys. Rev. Lett.* **67** 512